Supplementary Information

A Comprehensive Investigation into Thermoelectric Properties of PEDOT:PSS/$Bi_{0.5}Sb_{1.5}Te_3$ Composites

Saeed Masoumi[1], Kuanysh Zhussupbekov[2], Nadezda Prochukhan[3], Michael A. Morris[3], and Amir Pakdel[1,*]

[1] Department of Mechanical, Manufacturing, and Biomedical Engineering, Trinity College Dublin, The University of Dublin, D02PN40, Dublin, Ireland

[2] School of Physics, CRANN and AMBER Research Centres, Trinity College Dublin, The University of Dublin, D02PN40, Dublin, Ireland

[3] School of Chemistry, CRANN and AMBER Research Centres, Trinity College Dublin, The University of Dublin, D02PN40, Dublin, Ireland

E-mail: pakdela@tcd.ie

Content

1. Fabrication process of PEDOT:PSS/BST composite thin films

2. Fabrication process of single and sequentially post-treated PEDOT:PSS/40 wt% BST thin films

3. Methodology of measuring thickness of thin films

4. Centrifugation and size separation of BST powders after ball milling process

5. Fabricated PEDOT:PSS/BST composite thin films and the effect of HCl rinsing

6. Microstructural and morphological characterization of pristine PEDOT:PSS/BST thin films

7. Series- and parallel-connection models of PEDOT:PSS/BST composite thin films

8. Variable range hopping (VRH) models for pristine PEDOT:PSS/BST thin films

9. Temperature dependence of TE properties in post-treated PEDOT:PSS/40 wt% BST thin films

10. Microstructural and morphological characterization of post-treated PEDOT:PSS/40 wt% BST thin films

1. Fabrication process of PEDOT:PSS/BST composite thin films

Figure S1(a) shows the fabrication process of PEDOT:PSS/BST thin film composites. **Figure S1(b, c)** show the stability of PEDOT:PSS/BST suspensions by aging for 1 year. They illustrate good stability without separation.

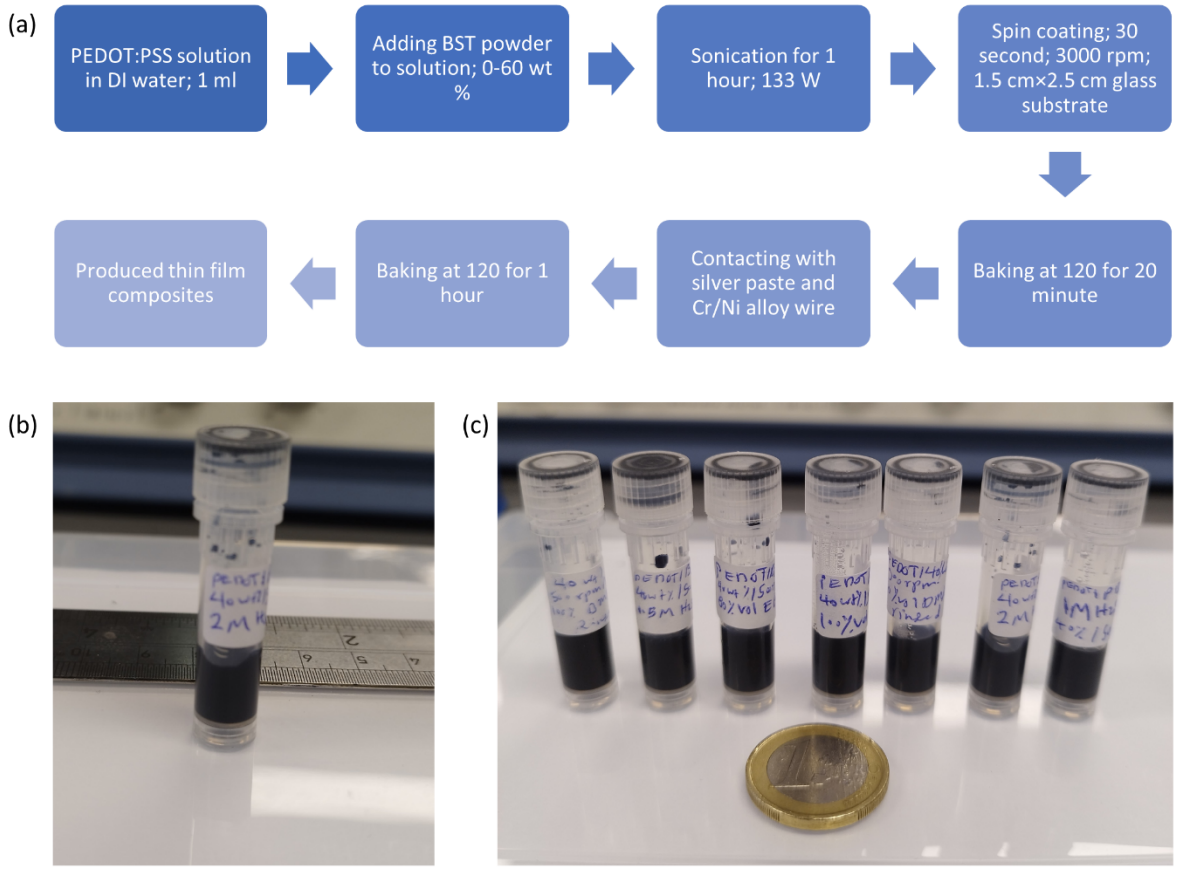

Figure S1. (a) The fabrication process of PEDOT:PSS/BST composite thin films, and (b, c) PEDOT:PSS/BST suspensions including 40 wt% of BST particles 12 months after preparation.

Figure S2(a, b) illustrate 200 µL of the PEDOT:PSS solutions that provides full surface coverage on the 15 mm × 25 mm glass substrate as well as spin coating machine. **Figure S2(c, d)** shows the fabricated pristine PEDOT:PSS thin film using solution diluted in DI water (0 vol% to 80 vol% of DI water) and recorded their room temperature resistance.

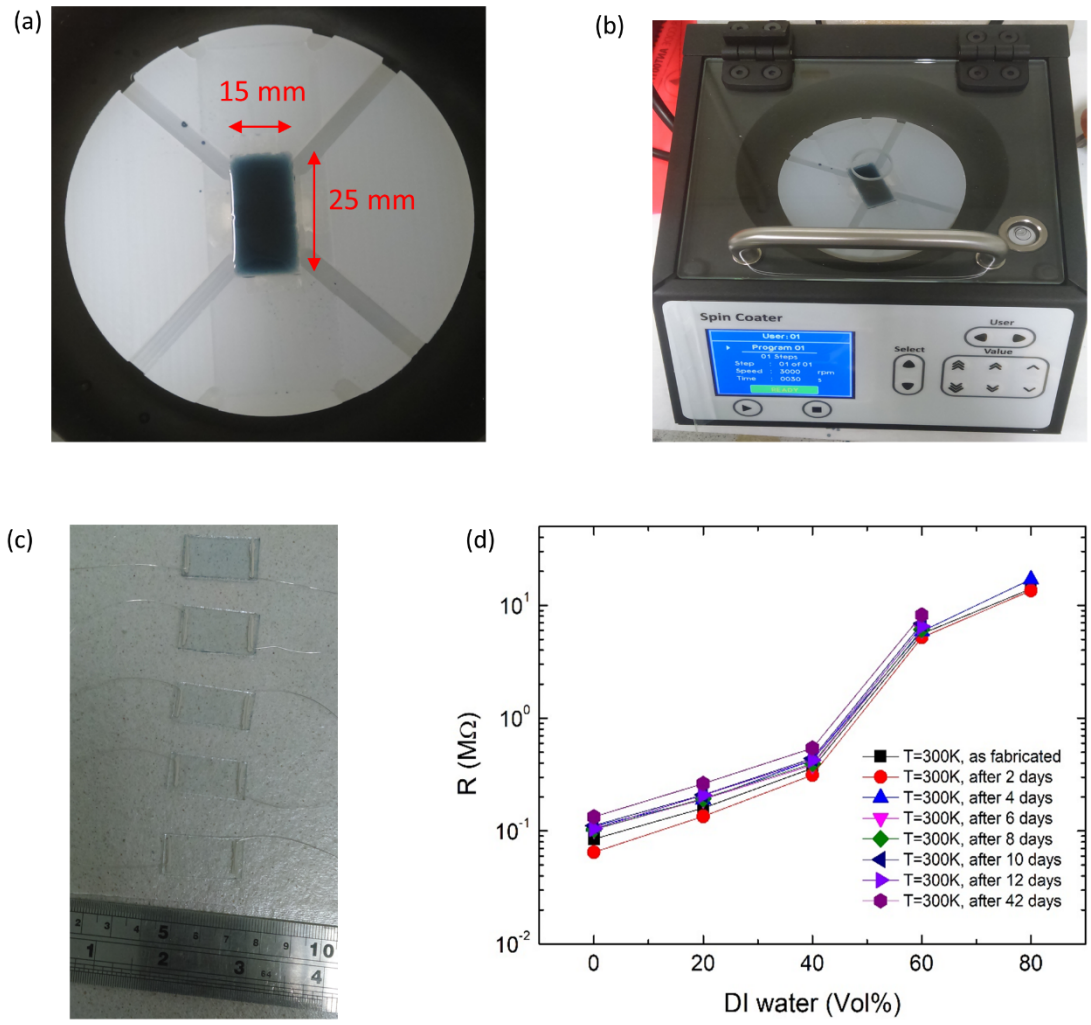

Figure S2. (a) 200 µl of the suspension fully covered the substrate. (b) Spin coating was performed at 3000 rpm for 30 seconds. (c) Wires were connected to the fabricated thin films using silver paste. (d) Room temperature resistance of the samples fabricated from the PEDOT:PSS suspension diluted in DI water.

2. Fabrication process of single and sequentially post-treated PEDOT:PSS/40 wt% BST thin films

Figure S3 shows the fabrication process of single post-treated PEDOT:PSS/40 wt% BST thin films. The treatment procedure is similar when employing DMSO and EG, but it is different for H_2SO_4 and NaOH. The last few steps however are similar for all treatment agents.

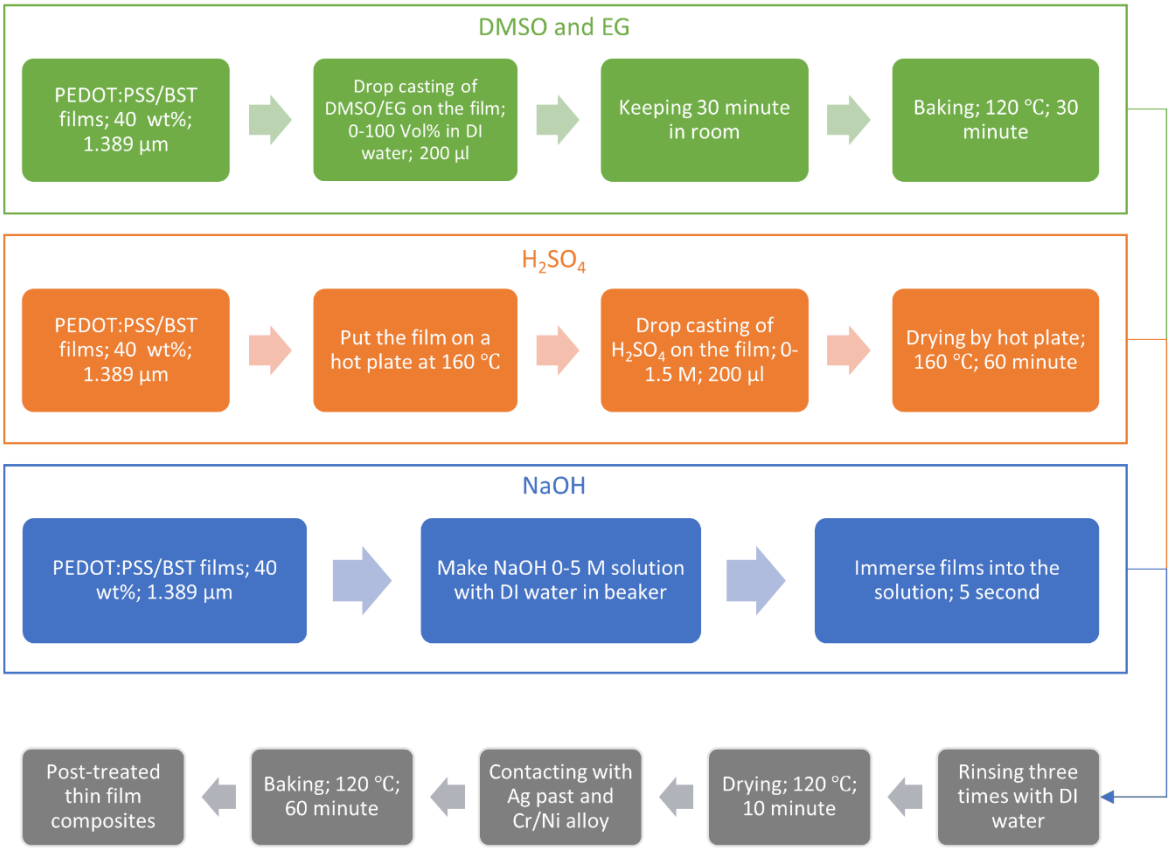

Figure S3. The fabrication process of single post-treating PEDOT:PSS/40 wt% BST thin film composites with DMSO, EG, H_2SO_4, and NaOH.

The process of rinsing composite thin films with DI water is schematically illustrated in **Figure S4(a)**. The rinsing process involved sequential immersing of thin films into three beakers containing DI water, using tweezers. This process was performed gently and slowly, always keeping the substrate and film in a horizontal position to minimize the potential BST particle loss during washing. To investigate the effect of rinsing with DI water on the number of BST particles, two similar composite thin films containing 20 wt% BST were fabricated. One thin film was subjected to rinsing with DI water three times, while no rinsing was performed on the other thin film. The surface morphologies of these two thin films were then analyzed using FE-SEM. Typical SEM micrographs of the two thin films are shown in **Figures S4(b)** and **(c)**. The SEM images did not indicate any significant changes in particle concentration and distribution in the samples with or without rinsing with DI water.

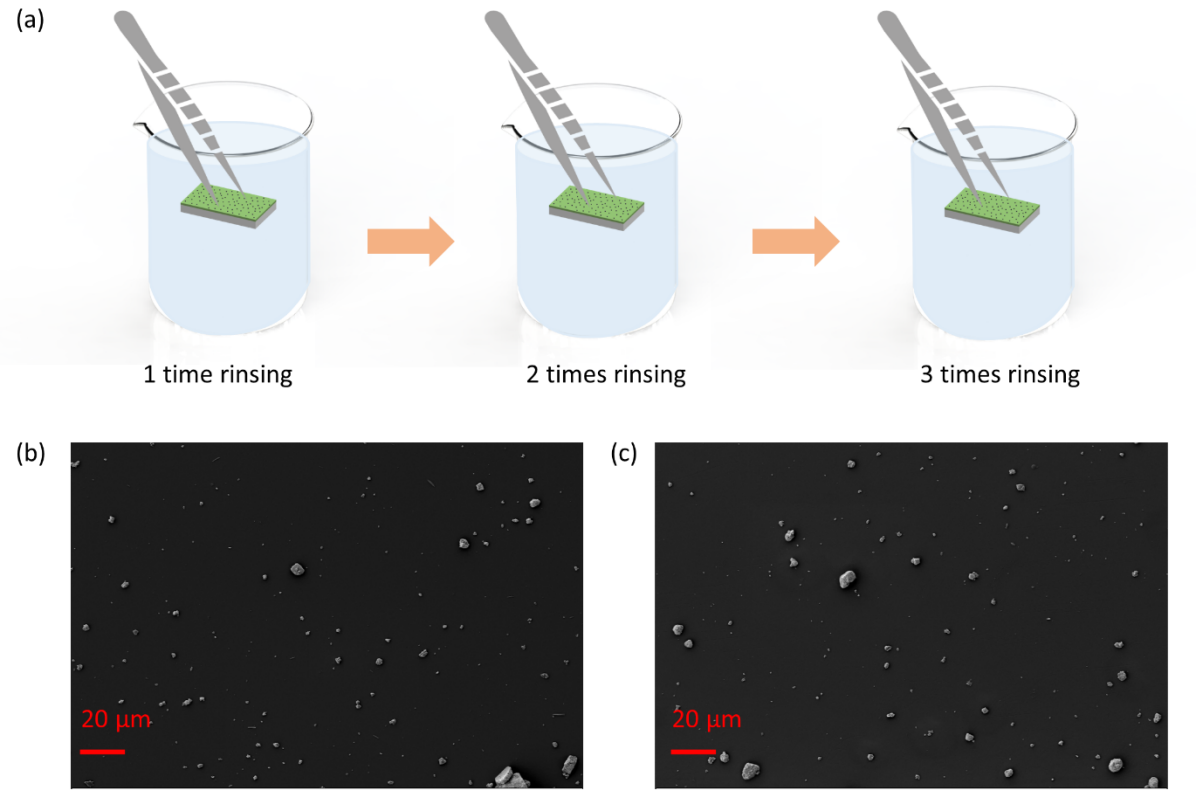

Figure S4. (a) Schematic diagram illustrating the process of rinsing post-treated thin films with DI water three times, and SEM micrographs of PEDOT:PSS/ 20 wt% BST (b) without and (c) with rinsing with DI water three times.

Figure S5 shows the fabrication process of sequential post-treatment in PEDOT:PSS/40 wt% BST thin films through several rounds of treatment with 40 vol% DMSO as well as post-treating with secondary dopants (DMSO, EG, and H_2SO_4) at optimum concentrations followed by post-treating with a chemical dedoping agent (NaOH) at different concentration from 0 M to 2 M.

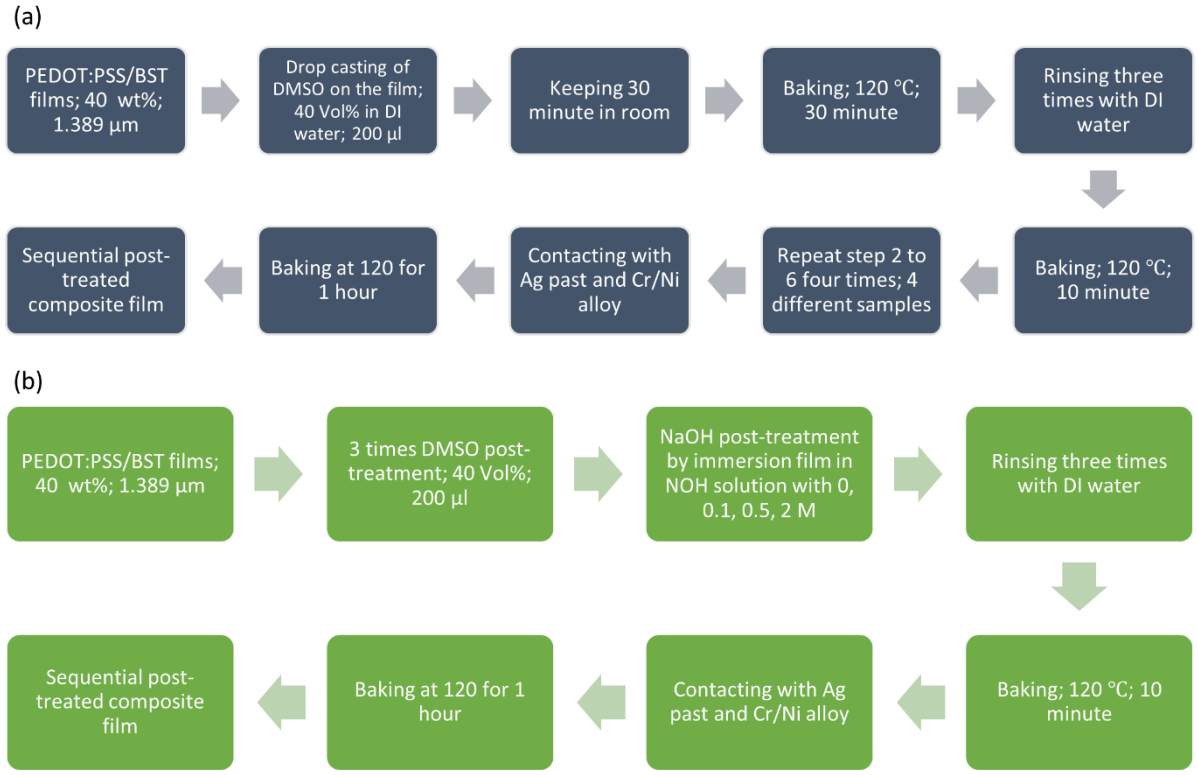

Figure S5. The fabrication process of sequential post-treating PEDOT:PSS/40 wt% BST thin film composites with (a) various number of 40 vol% DMSO, and (b) both secondary and chemical dedoping including 40 vol% DMSO-NaOH, 40 vol% EG-NaOH, and 0.5 M H_2SO_4-NaOH.

3. Methodology of measuring thickness of thin films

Figure S6 shows 3D and 2D schematics of the thickness measurement process in composite thin films containing BST particles, focusing on typical step-height profiles within a defined area of 20 µm × 20 µm using AFM. Firstly, a composite thin film was selected for thickness measurement, as shown in **Figure S6(a)**. A scratch line was then made on the surface of the polymeric films to create a step-height consisting of the film surface and the glass substrate, as shown in **Figure S6(b)**. The magnified illustration of this step-height edge (area A) is shown in **Figure S6(c)**. AFM was subsequently used to scan an area of 20 µm × 20 µm containing the step-height, as depicted in **Figure S6(d)**. Finally, typical step-height profiles were obtained within the scanned area of 20 µm × 20 µm at clean and smooth edges to ensure consistency and accuracy in measuring the thickness of the matrix material (i.e., PEDOT:PSS). This explains the discrepancy between the reported film thickness values (~100 nm range) and the average particle size values (~1.3 µm range).

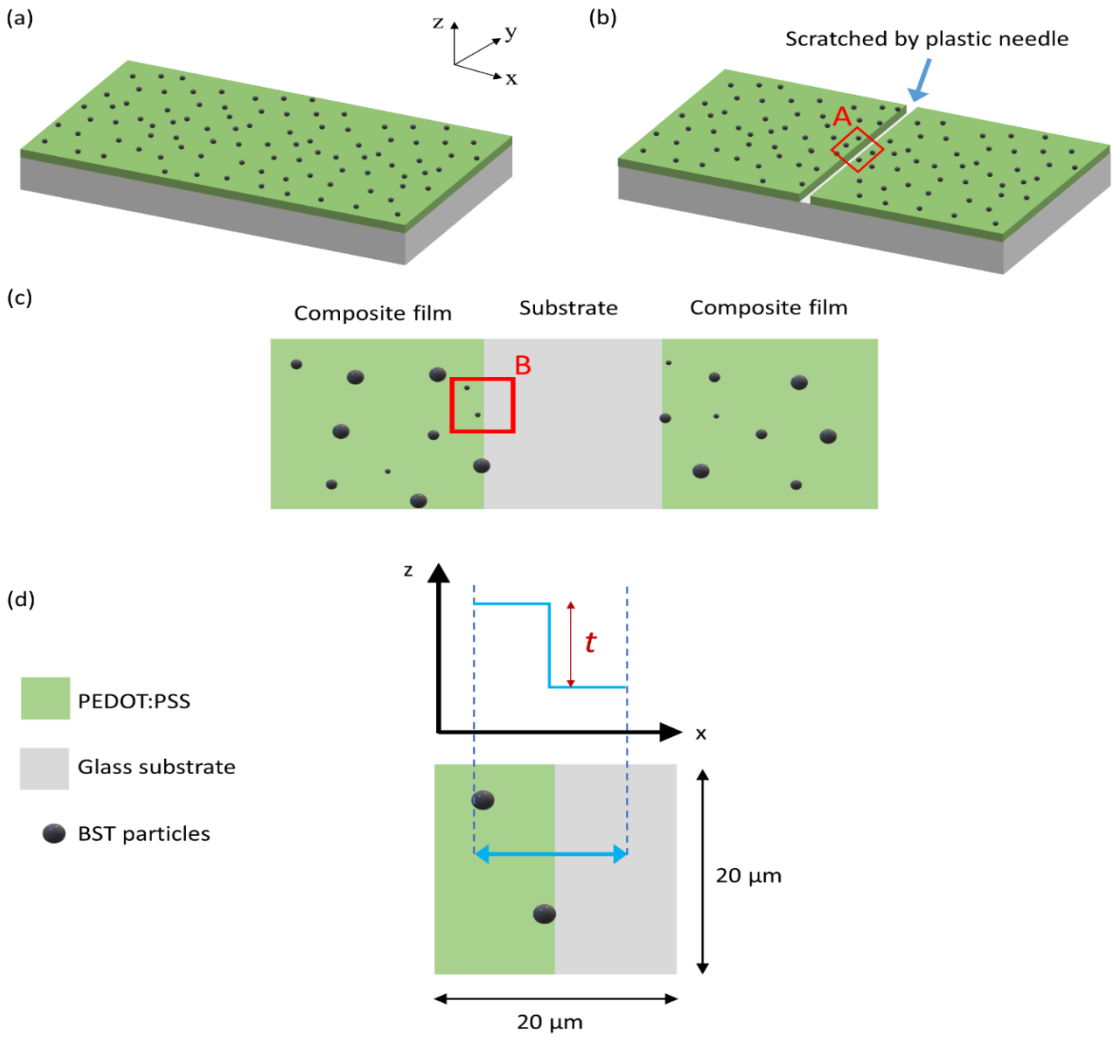

Figure S6. Schematic diagram illustrating the process of thickness (t) measurement with AFM through typical step-height profile. (a) PEDOT:PSS/BST composite thin films, (b) scratched the surface of composite thin film by plastic needle, (c) the magnified illustration of area A in (b), and (d)) the magnified illustration of area B in (c) in 2D view that shows the typical step-height profile and thickness of the composite thin film.

4. Centrifugation and size separation of BST powders after ball milling process

Figures 7-9 display the SEM micrographs, particle distributions, and the minimum, maximum, and average particle sizes obtained from Set1, Set3, and Set4 centrifugation procedures. Set1 resulted in average particle sizes of 1.785 µm, 467 nm, and 450 nm for centrifugation speeds of 500 rpm, 1000 rpm, and 5000 rpm, respectively. Set3 centrifugation yielded particle sizes of 1.413 µm, 550 nm, and 436 nm at speeds of 250 rpm, 500 rpm, and 8000 rpm, respectively. Similarly, Set4 centrifugation produced average particle sizes of 249 nm, 155 nm, and 119 nm for centrifugation speeds of 2000 rpm, 5000 rpm, and 9000 rpm, respectively.

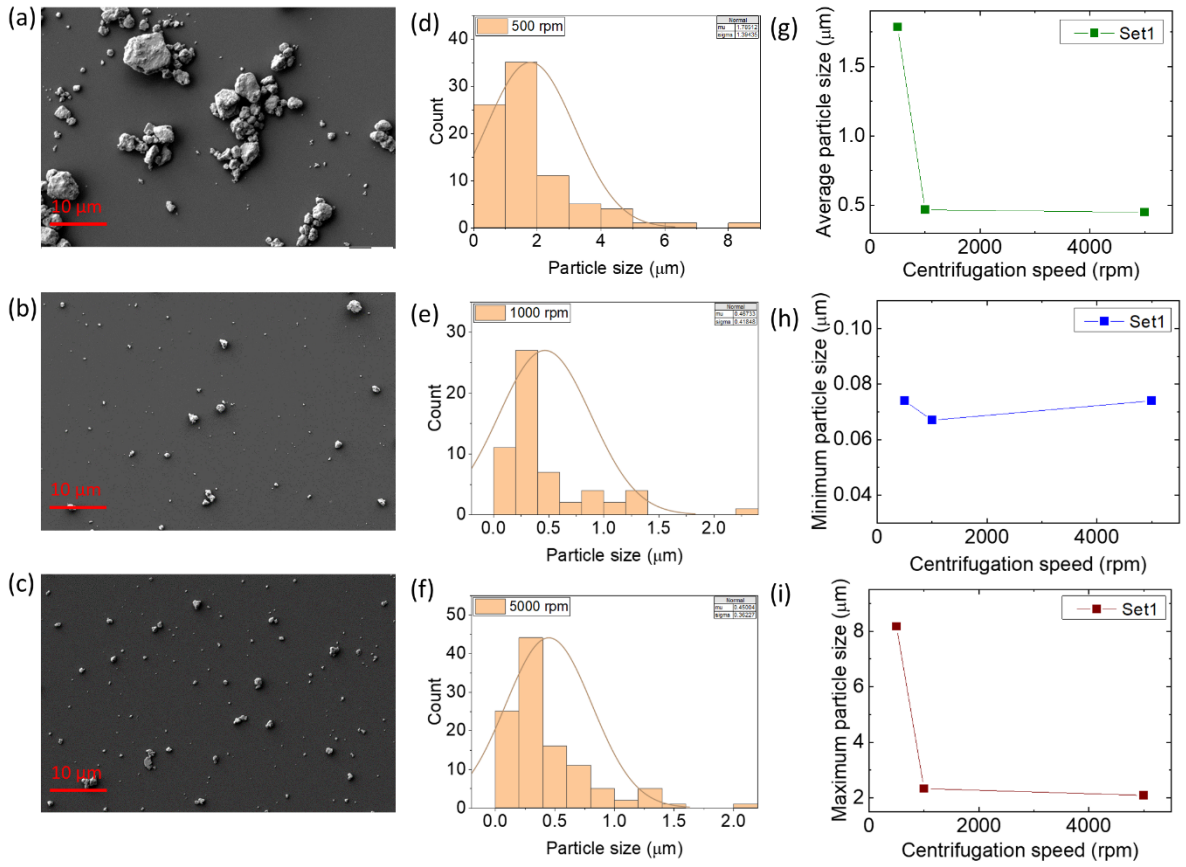

Figure S7. SEM micrograph and particle size distribution of BST powder centrifuged by Set1 procedure at three different speeds for 2 minutes: (a, d) 500 rpm, (b, e) 1000 rpm, and (c, f) 5000 rpm. The variation of (g) average, (h) minimum, and (i) maximum particle size of BST powder with centrifugation speed.

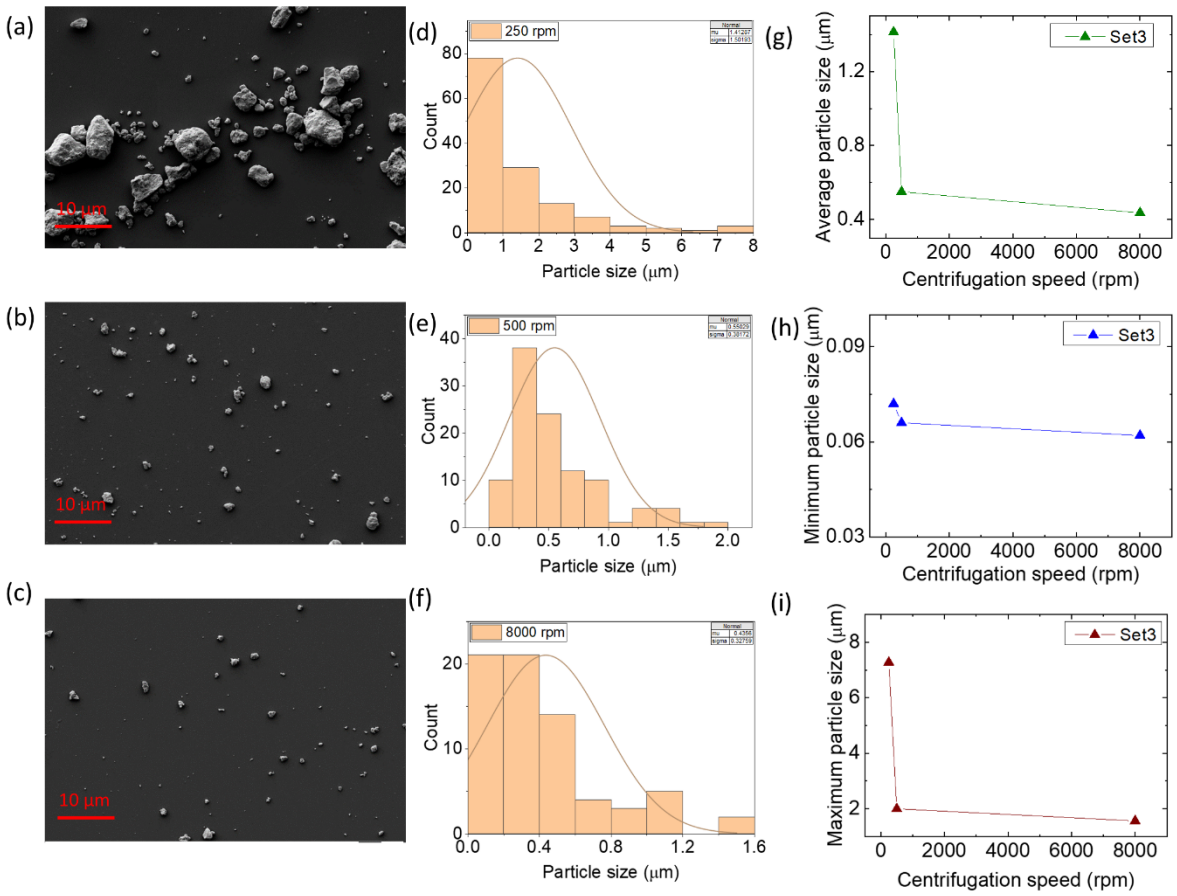

Figure S8. SEM micrograph and particle size distribution of BST powder centrifuged by Set3 procedure at three different speeds sequentially for 2 minutes: (a, d) 250 rpm, (b, e) 500 rpm, and (c, f) 8000 rpm. The variation of (g) average, (h) minimum, and (i) maximum particle size of BST powder with centrifugation speed.

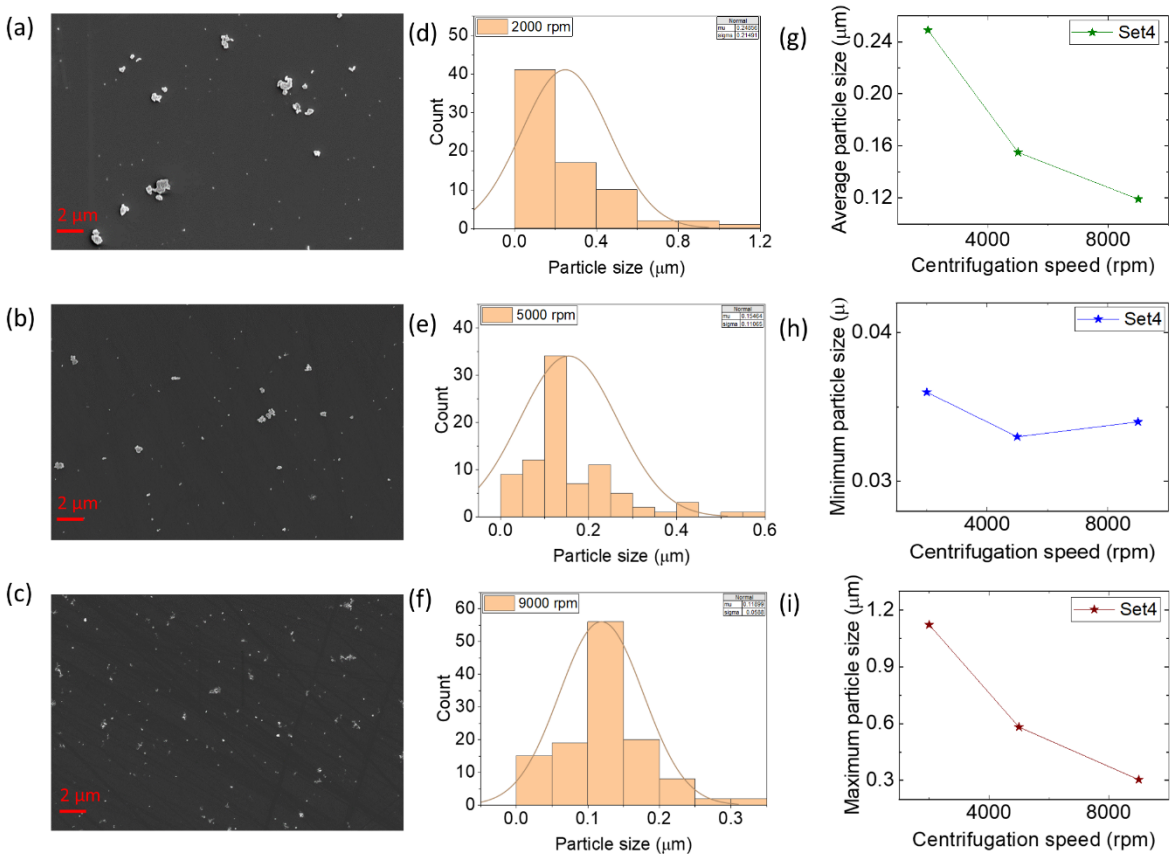

Figure S9. SEM micrograph and particle size distribution of BST powder centrifuged by Set4 procedure at three different speeds sequentially for 2 minutes: (a, d) 2000 rpm, (b, e) 5000 rpm, and (c, f) 9000 rpm. The variation of (g) average, (h) minimum, and (i) maximum particle size of BST powder with centrifugation speed.

5. Fabricated PEDOT:PSS/BST composite thin films and the effect of HCl rinsing

Figure S10 illustrates the fabricated PEDOT:PSS/BST thin film composites containing 0-60 wt% of BST particle with the size of 1.389 µm, 40 wt% BST with four different particle sizes as well as 40 wt% BST with the particle size of 1.389 µm that rinsed with HCl and without rinsing. **Figure S11** illustrate the variation of σ, S, and PF of PEDOT:PSS/BST thin film composites with BST particles that rinsed with HCl and without rinsed. This figure shows the effect of HCl rinsing on TE properties of thin film composites that the HCl rinsing improve the PF of PEDOT:PSS/BST thin film composites.

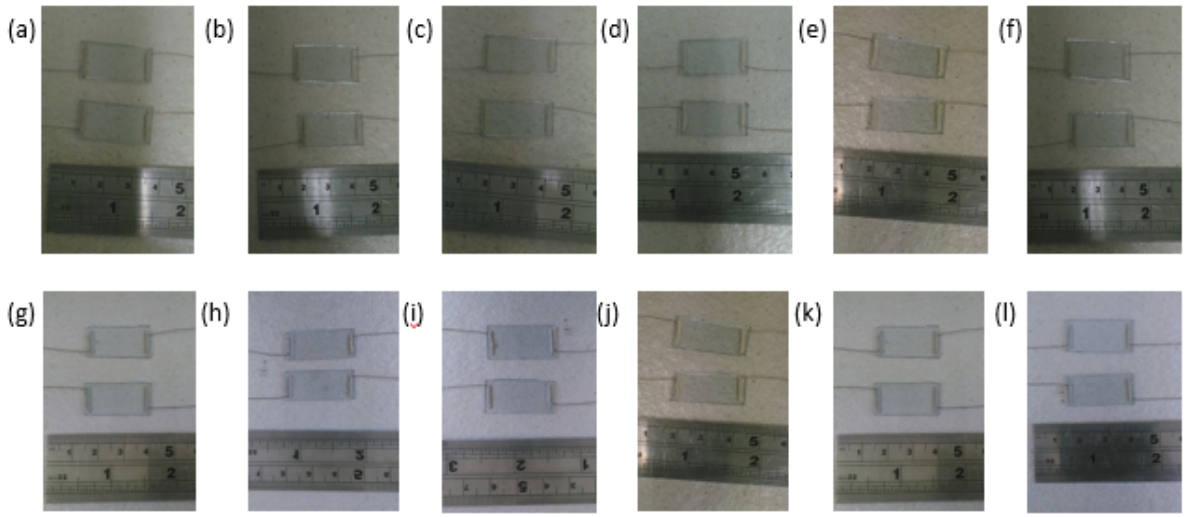

Figure S10. The fabricated PEDOT:PSS/BST thin film composites, BST particle concentration of (a) 0 wt%, (b) 5 wt%, (c) 10 wt%, (d) 20 wt%, (e) 40 wt%, (f) 60 wt% with the size of 1.389 µm, and 40 wt% BST particle with the size of (g) 1.389 µm, (h) 0.792 µm, (i) 429 nm, (j) 316 nm, and 40 wt% BST particle with the size of 1.389 µm (k) rinsed by HCl and (l) without rinsing.

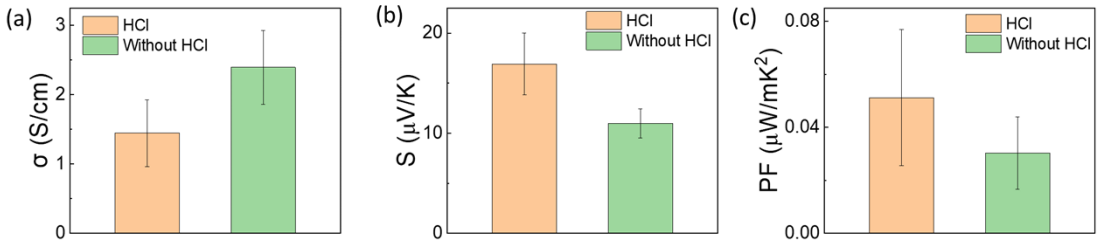

Figure S11. The variation of (a) σ, (b) S, and (c) PF of PEDOT:PSS/BST thin film composites with BST particles that rinsed with HCl and without rinsed. The error bars were calculated by three times repetition of measurements on two set of samples.

6. Microstructural and morphological characterization of pristine PEDOT:PSS/BST thin films

Typical SEM micrographs, AFM topography images and step-height profiles of PEDOT:PSS and PEDOT:PSS/BST thin films are presented in **Figures S12-S15**.

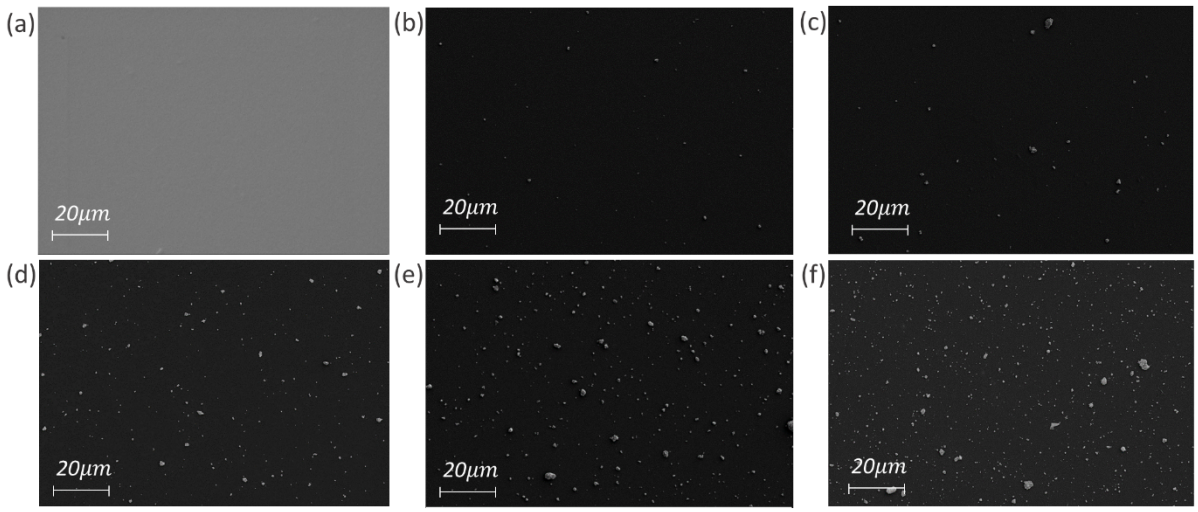

Figure S12. SEM micrograph of pristine PEDOT:PSS/BST composite thin films, (a) 0 wt%, (b) 5 wt%, (c) 10 wt%, (d) 20 wt%, (e) 40 wt%, and (f) 60 wt% BST powder with an average particle size of 1.389 μm.

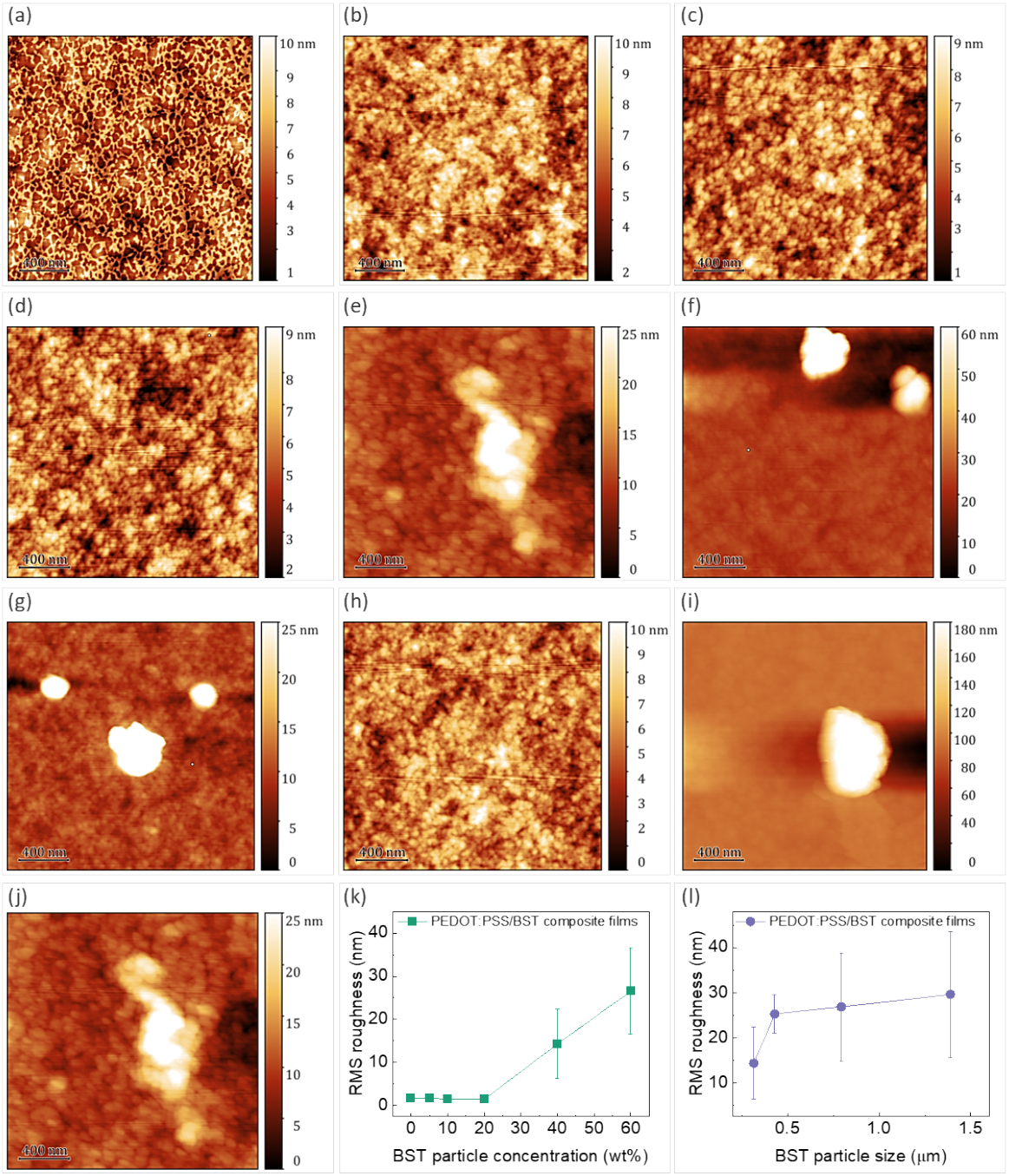

Figure S13. AFM images of pristine PEDOT:PSS/BST thin film composites containing (a) 0 wt%, (b) 5 wt%, (c) 10 wt%, (d) 20 wt%, (e) 40 wt%, (f) 60 wt%, and PEDOT:PSS/40 wt% BST thin film composites with the BST particle size of (g) 1.389 μm, (h) 0.792 μm, (i) 429 nm, (j) 316 nm, the RMS roughness of the samples vs BST (k) concentration, and (l) size. All the scan areas are: 2 × 2 μm^2. The error bars in (g) and (h) were calculated using RMS values obtained from two different AFM images, with scan areas of 2 × 2 μm^2 and 5 × 5 μm^2.

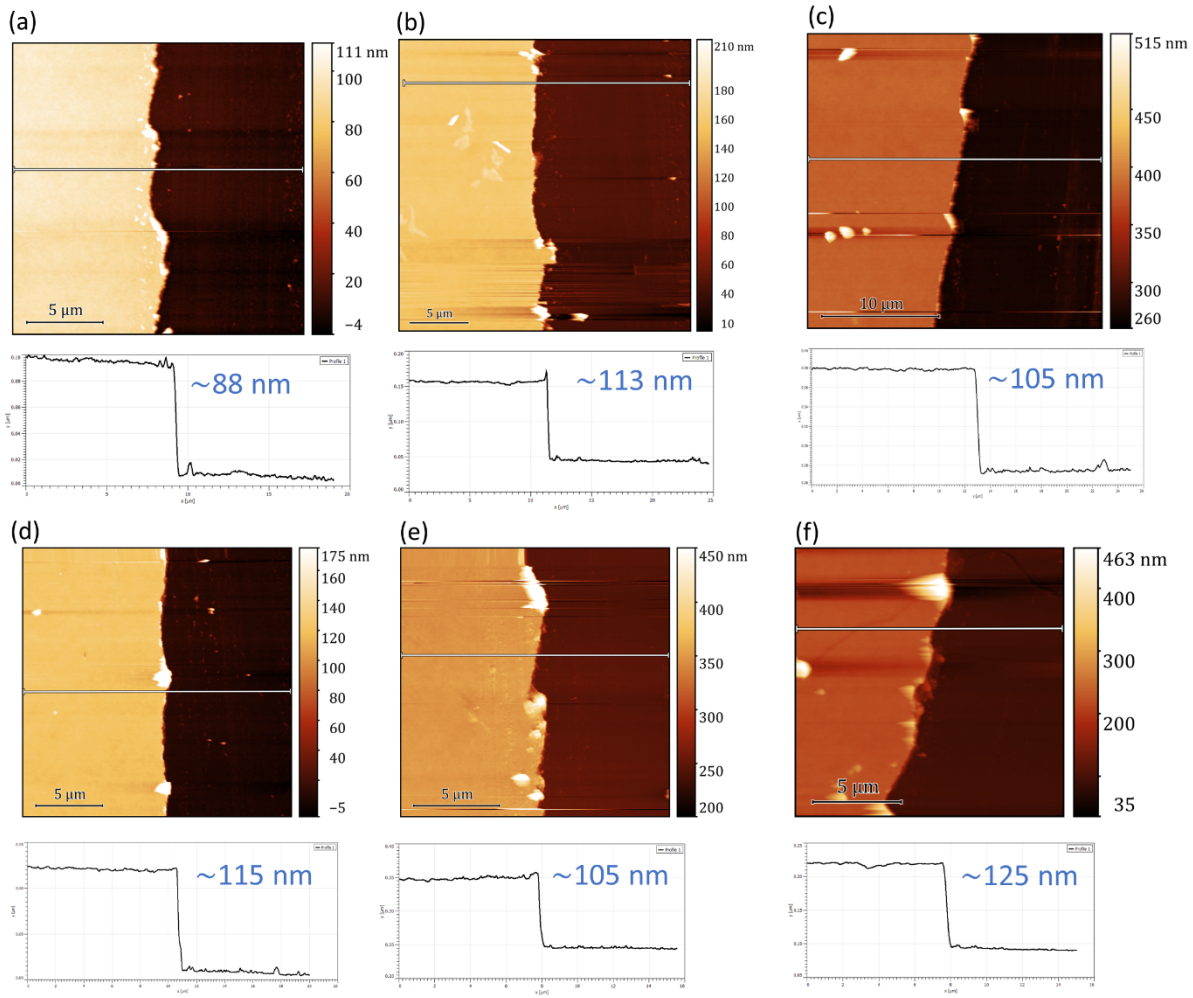

Figure S14. Typical step-height profile (film thickness (*t*)) measured with AFM (Asylum MFP-3D microscope with AC Air Topography mode; scanning at 308 kHz frequency; using rectangular cantilevers with tetrahedral tips from Oxford Instruments) for the pristine PEDOT:PSS/BST thin film composites, (a) 0 wt%, (b) 5 wt%, (c) 10 wt%, (d) 20 wt%, (e) 40 wt%, and (f) 60 wt%.

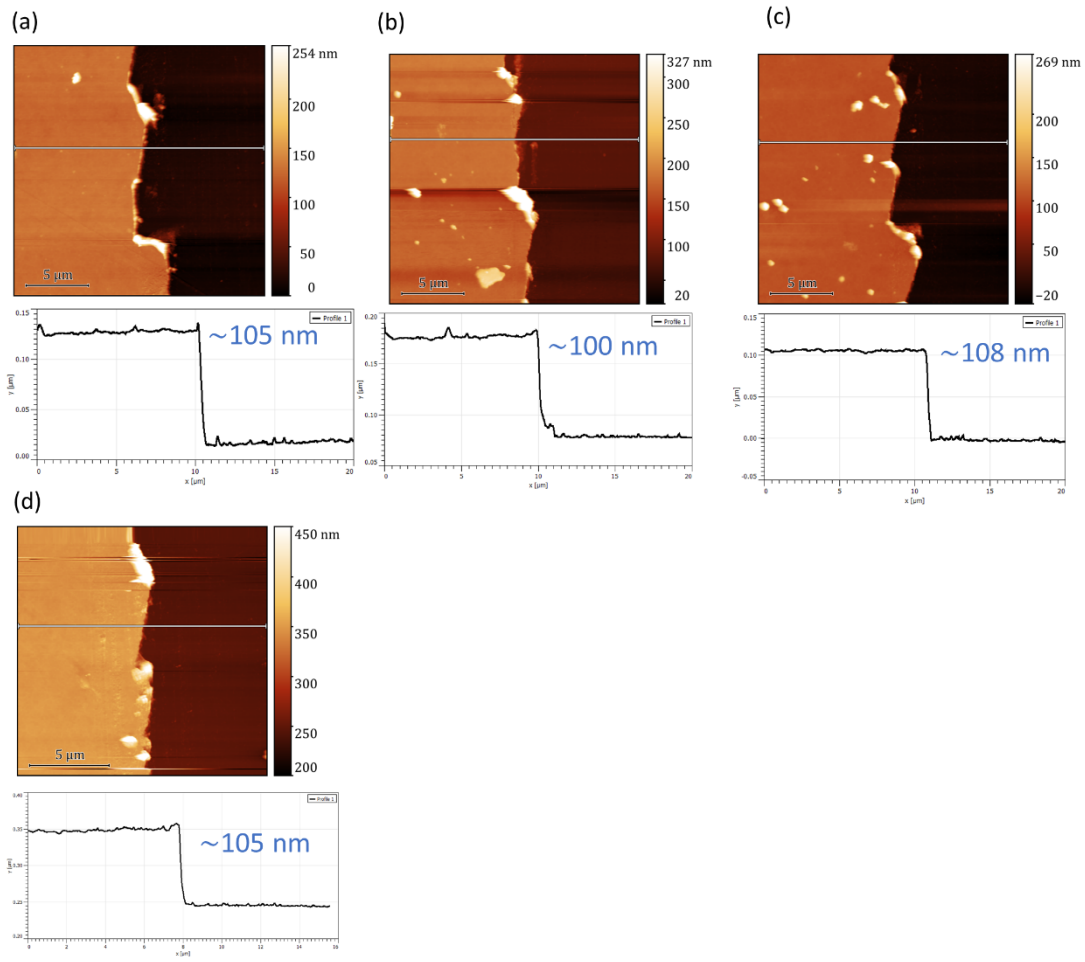

Figure S15. Typical step-height profile (film thickness (*t*)) and surface topography for the pristine PEDOT:PSS/40 %wt BST thin film composites with BST particle sizes of (a) 1.389 µm, (b) 0.792 µm, (c) 429 nm, and (d) 316 nm.

7. Series- and parallel-connection models of PEDOT:PSS/BST composite thin films

The PEDOT:PSS used in this work had a solid content of 1.0 - 1.2% (approximately 1.1%) with a density of 0.999 g/cm³ in dried coatings. Therefore, the weight of PEDOT:PSS in a 1 mL solution was 11 mg. The BST in this study had a density of 6.75 g/cm³. The volume fractions of BST fillers were calculated based on the densities of PEDOT:PSS and BST, as well as the wt% of the BST fillers. The results are presented in **Table S1**. The thermoelectric (TE) properties of PEDOT:PSS and BST were obtained from reference [1] and the datasheet from Thermonamic Electronics (Jiangxi) Corp., Ltd., respectively. The TE data are presented in **Table S2**, which is used for the series- and parallel-connection models."

Table S1. Volume and weight ratio of BST filler in the composite.

wt% of BST	0	5	10	20	40	60
mg of BST	0	0.55	1.1	2.2	4.4	6.6
vol% of BST	0	0.77	1.62	3.57	8.98	18.17
Composite density (g/cm³)	0.999	1.04	1.09	1.2	1.52	2.04

Table S2. TE properties of filler (F; BST) and matrix (M; PEDOT:PSS).

σ_F (S/cm)	σ_M (S/cm)	S_F (μV/K)	S_M (μV/K)	k_F (W/mK)	k_M (W/mK)
1050	1.3	215	15.4	1.4	0.25

8. Variable range hopping (VRH) models for pristine PEDOT:PSS/BST thin films

Figure S16 shows the temperature dependency of electrical conductivity and Seebeck coefficient with the linear fitting to the Mott VRH model of the experimental data. According to equations (5) and (6), ln σ as a function of $T^{-1/4}$ and S as a function of $T^{1/2}$ were plotted for pristine PEDOT:PSS/BST thin film composites with various concentrations of (a, d) 10 wt.%, (b, e) 20 wt.%, (c, f) 60 wt.% of BST particles. The dash lines show the linear fitting to the Mott VRH model based on equation (5) and (6) in the manuscript.

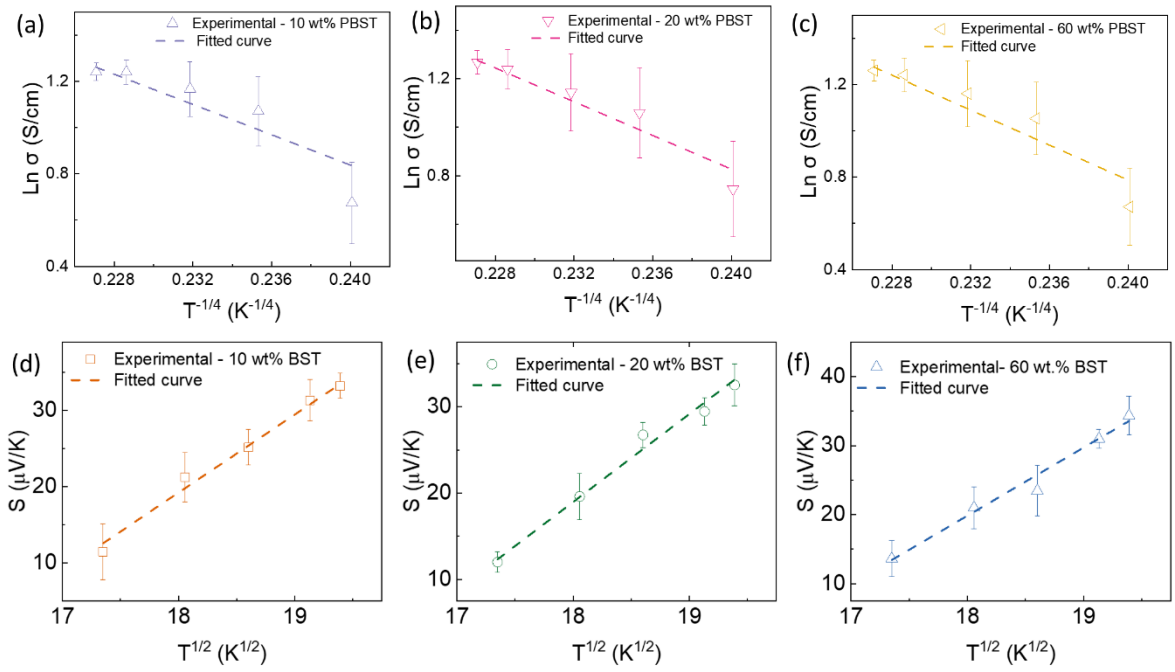

Figure S16. ln σ as a function of $T^{-1/4}$ and S as a function of $T^{1/2}$ for pristine PEDOT:PSS/BST thin film with various concentrations of (a, d) 10 wt.%, (b, e) 20 wt.%, (c, f) 60 wt.% of BST particles. The dashed lines in show the linear fitting to the Mott VRH model of the experimental data. The error bars on experimental data were calculated by three time repetitions of measurements on two sets of samples.

9. Temperature dependence of TE properties in post-treated PEDOT:PSS/40 wt% BST thin films

Figure S17 illustrates the temperature dependence of electrical conductivity and Seebeck coefficient for PEDOT:PSS/40 wt.% BST thin films. The samples were single post-treated with various concentrations of EG and NaOH, sequentially post-treated with 40 vol% DMSO (1-4 rounds), and 40 vol% EG-NaOH. The results reveal metallic temperature dependency for both electrical conductivity and Seebeck coefficient in the thin films. However, the NaOH single post-treated samples exhibited both metallic and semiconducting temperature-dependent behaviour in their electrical conductivity, while showing metallic temperature dependency in their Seebeck coefficient. Additionally, the dashed lines in **Figure S17(e-h)** represent the linear fitting of equation (7) to the experimental data of the Seebeck coefficient for all post-treated samples. The error bars on the experimental data were calculated based on three repetitions of electrical conductivity and Seebeck coefficient measurements on the samples.

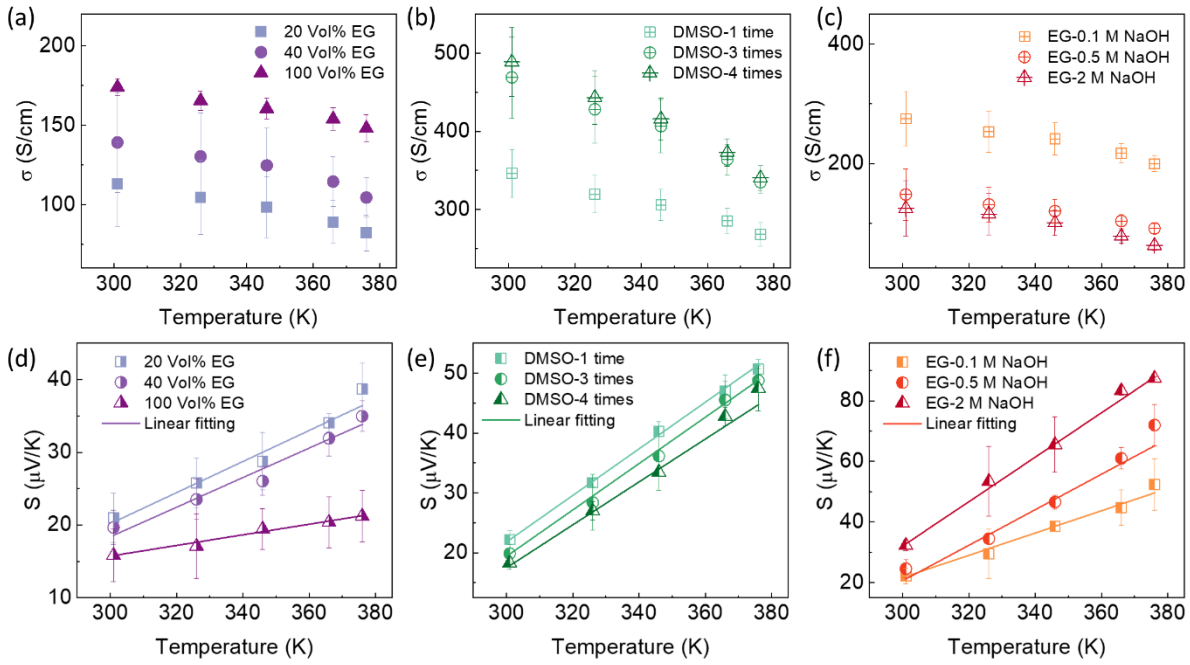

Figure S17. The variation of electrical conductivity and Seebeck coefficient with temperature for PEDOT:PSS/ 40 wt.% BST thin film composites single post-treated with (a, d) EG, sequentially post-treated with (b, e) 40 vol% DMSO with different numbers of post-treatment, and (c, f) 40 vol% EG-NaOH. The dash lines in Figure S17(d-f) show the linear fitting of equation (7) to the experimental data. The error bars on experimental data were calculated by three times repetition of measurements on the samples.

10. Microstructural and morphological characterization of post-treated PEDOT:PSS/40 wt% BST thin films

The thicknesses and surface topology of the single and sequentially post-treated thin films with DMSO, EG, H_2SO_4, and NaOH were measured by AFM. Surface topology images of the composite thin films after single and sequential post-treatments with DMSO, EG, H_2SO_4, and NaOH are illustrated in Supporting Information **Figures S18** and **S19**, respectively.

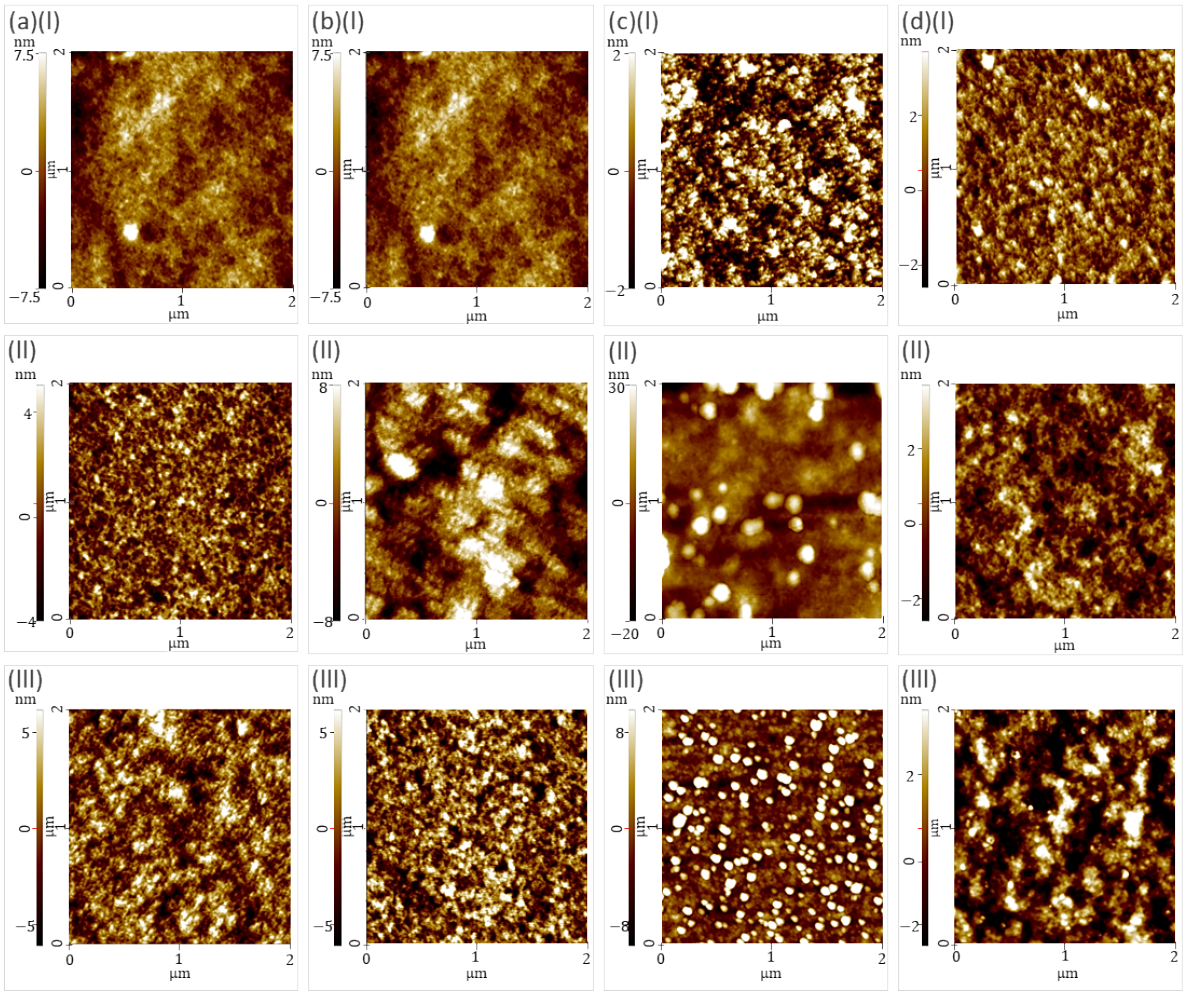

Figure S18. The surface topography of single post-treated PEDOT:PSS/40 wt% BST thin films with (a) DMSO: (I) 0 vol%, (II) 20 vol%, (III) 100 vol%; (b) EG: (I) 0 vol%, (II) 20 vol%, (III) 100 vol%; (c) H_2SO_4: (I) 0 M, (II) 0.5 M, (III) 1.5 M; and (d) NaOH; (I) 0 M, (II) 0.5 M, (III) 5 M. All the surface scan areas for topography images are: 2 × 2 µm^2.

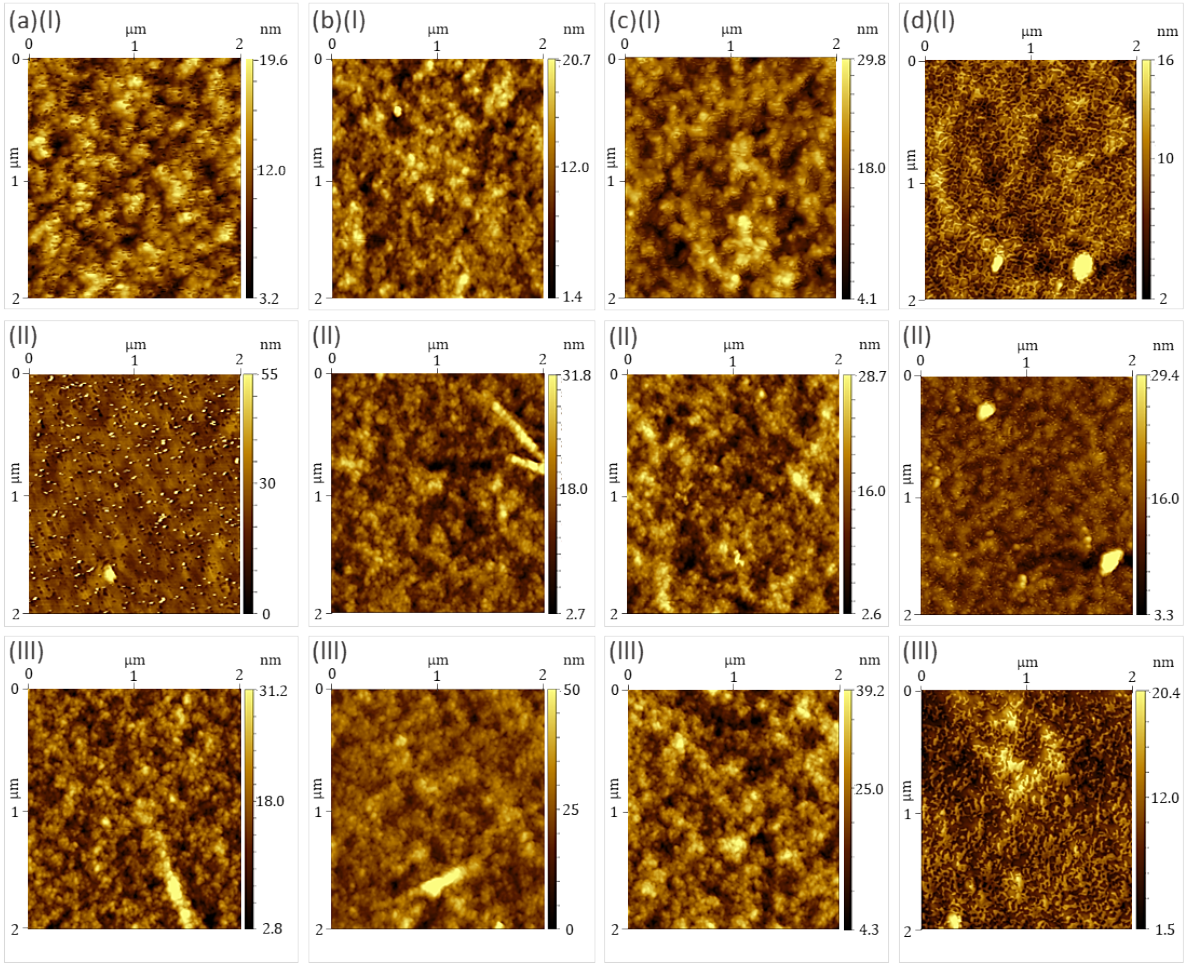

Figure S19. The surface topography of single post-treated PEDOT:PSS/40 wt% BST thin films with (a) DMSO: (I) 1 round, (II) 3 rounds, (III) 4 rounds; (b) 40 vol% DMSO-X M NaOH, (c) 40 vol% EG-X M NaOH, and (d) 0.5 M H_2SO_4-X M NaOH; X = 0 M (I), 0.1 M (II), 2M (III). All the surface scan areas for topography images are: 2 × 2 µm^2.

The step-height profile of the post-treated thin films was used to calculate the thicknesses of the thin films, as shown in **Figures S20** and **S21**. The average thicknesses of single post-treated thin films with DMSO, EG, H_2SO_4, and NaOH were 75 nm, 91 nm, 64 nm, and 56 nm, respectively. Additionally, the thickness of post-treated thin films decreased with EG concentration, while it increased with NaOH concentration. However, the film thicknesses remained almost constant with the number of post-treatment rounds using 40 vol% DMSO, where the average thickness of sequential post-treated samples was 44 nm. Similarly, the thicknesses of 40 vol% DMSO-NaOH, 40 vol% EG-NaOH, and 0.5 M H_2SO_4-NaOH thin films were almost constant with NaOH concentration, measuring an average of 42 nm, 40 nm, and 40 nm, respectively.

Compared with the pristine thin film, most single post-treated films with a secondary dopant experienced a decrease in thickness. This could be attributed to the induction of a screening effect due to the high dielectric constant and polarity of the post-treatment solutions, weakening the PEDOT-PSS coulombic force, removing some PSS, and consequently reducing the film thickness. This is in agreement with findings demonstrated in the literature. The removal of excessive insulating PSS domains establishes an interconnected network between the conducting PEDOT chains, facilitating the unimpeded transmission of carriers and resulting in high electrical conductivity.

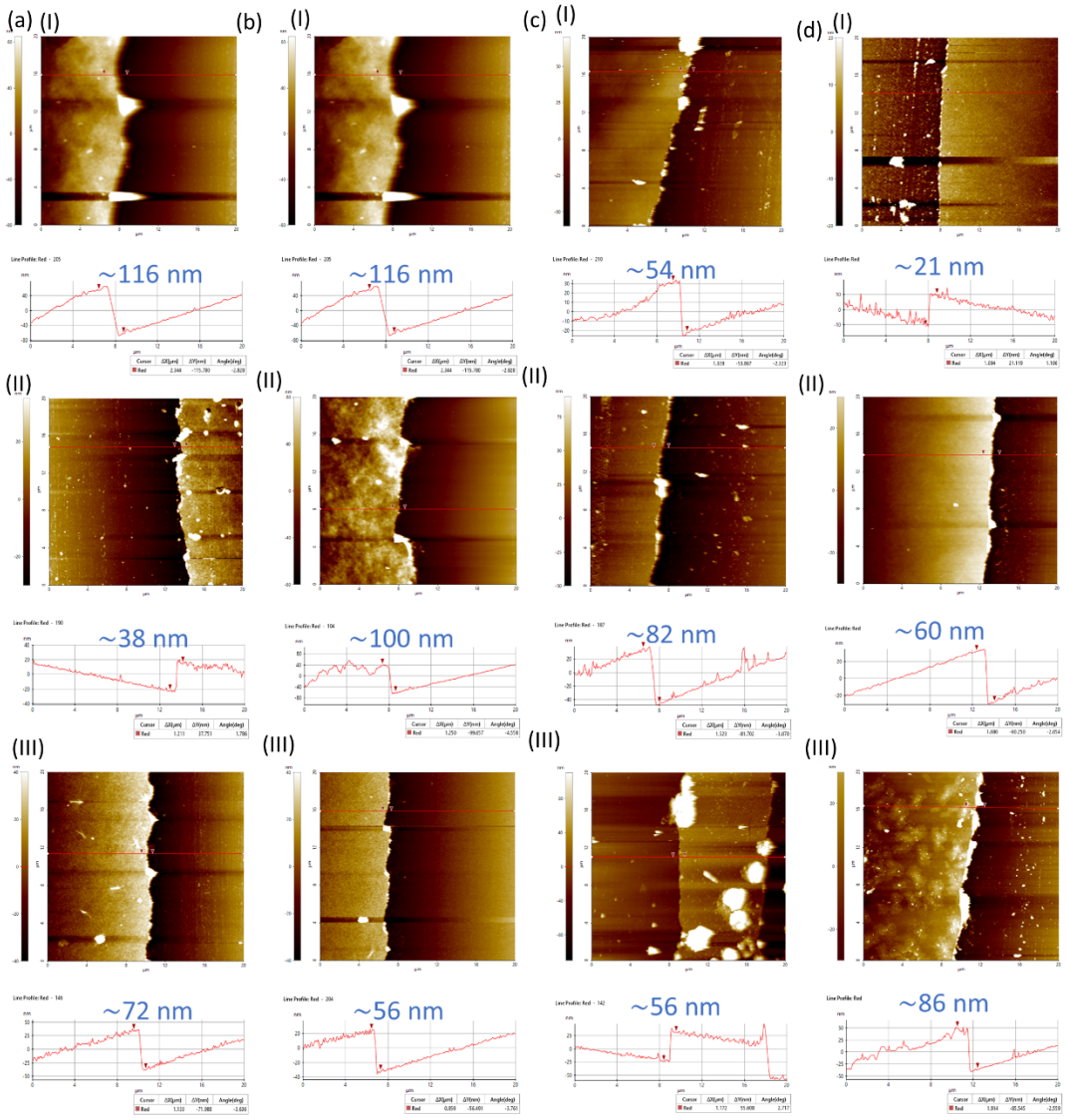

Figure S20. Typical step-height profile (film thickness (*t*)) and surface topography of single post-treated PEDOT:PSS/40 wt% BST thin film composites, (a) DMSO; (I) 0 vol%, (II) 20 vol%, and (III) 100 vol%, (b) EG; (I) 0 vol%, (II) 20 vol%, and (III) 100 vol%, (c) H_2SO_4; (I) 0 M, (II) 0.5 M, and (III) 1.5 M, and (d) NaOH; (I) 0 M, (II) 0.5 M, and (III) 5 M.

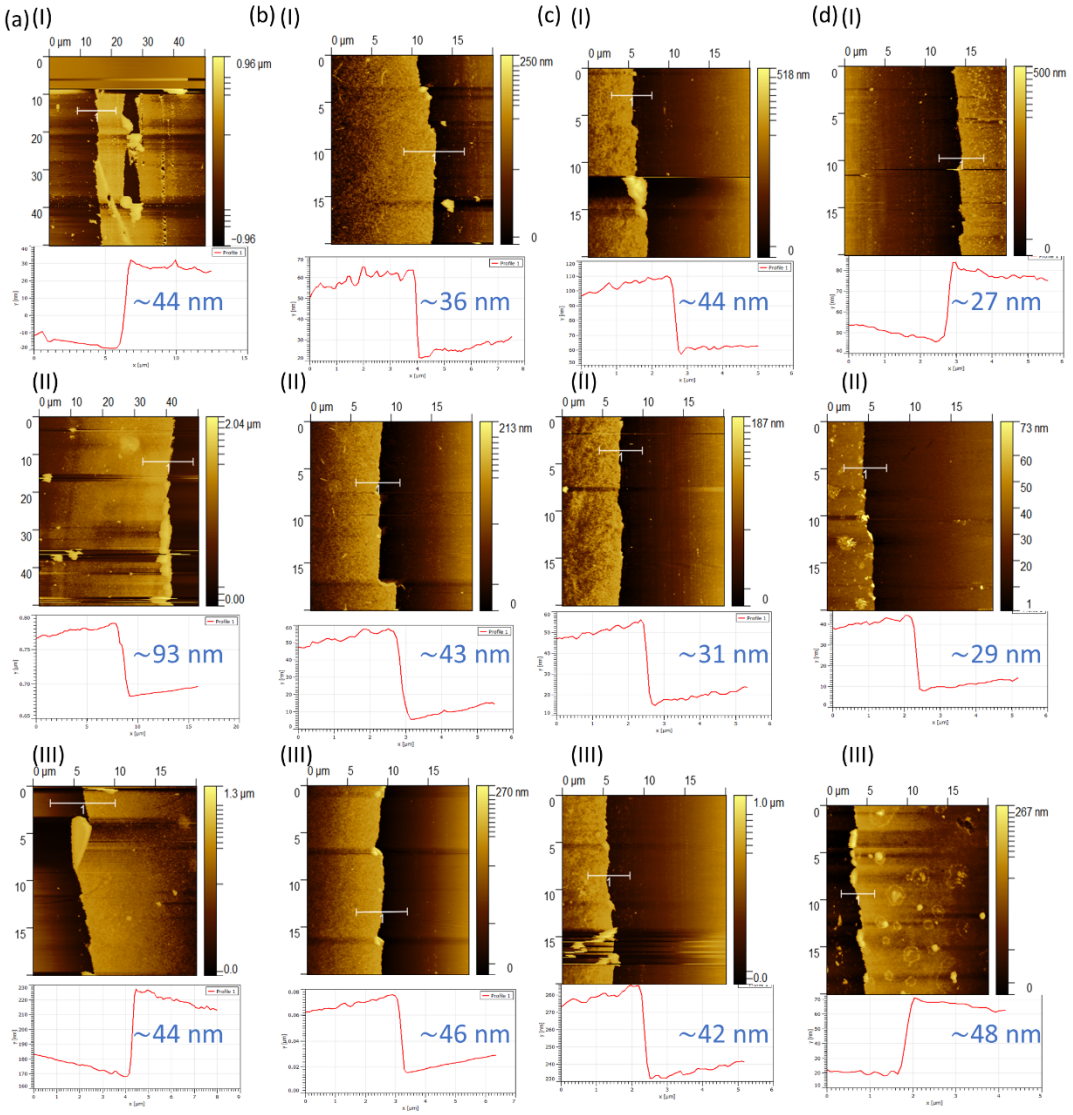

Figure S21. Typical step-height profile (film thickness (*t*)) and surface topography of sequentially post-treated PEDOT:PSS/40 wt% BST thin film composites, (a) 40 vol% DMSO; (I) 1 time, (II) 3 times, and (III) 4 times, (b) 40 vol% DMSO-NaOH, (c) 40 vol% EG-NaOH, and (d) H_2SO_4-NaOH; (I) 0 M, (II) 0.1 M, and (III) 2 M of NaOH.

The effect of BST particles on the overall structure of PEDOT:PSS thin films were analysed through XRD characterization on the BST powder, pristine PEDOT:PSS and PEDOT:PSS/40 wt% BST films, and 0.5 M H_2SO_4-0.1 M NaOH post-treated PEDOT:PSS and PEDOT:PSS/40 wt% BST films. In order to further analysis, SAXS and WAXS characterization were also performed on the polymeric thin films. The patterns of characterizations are shown in **Figure S22(a-d)**.

In **Figure S22(d)**, a characteristic peak with q = 0.3 $Å^{-1}$ (d = 20.9 Å calculated with d = 2π/q) is attributed to alternating stacking of PEDOT and PSS (i.e., PEDOT (100) crystal planes). The lattice spacing distance of (100) plane (d_{100}) for PEDOT:PSS is 20.9 Å, which is almost similar in four polymeric thin films. This is consistent with the reported value in literature [2].

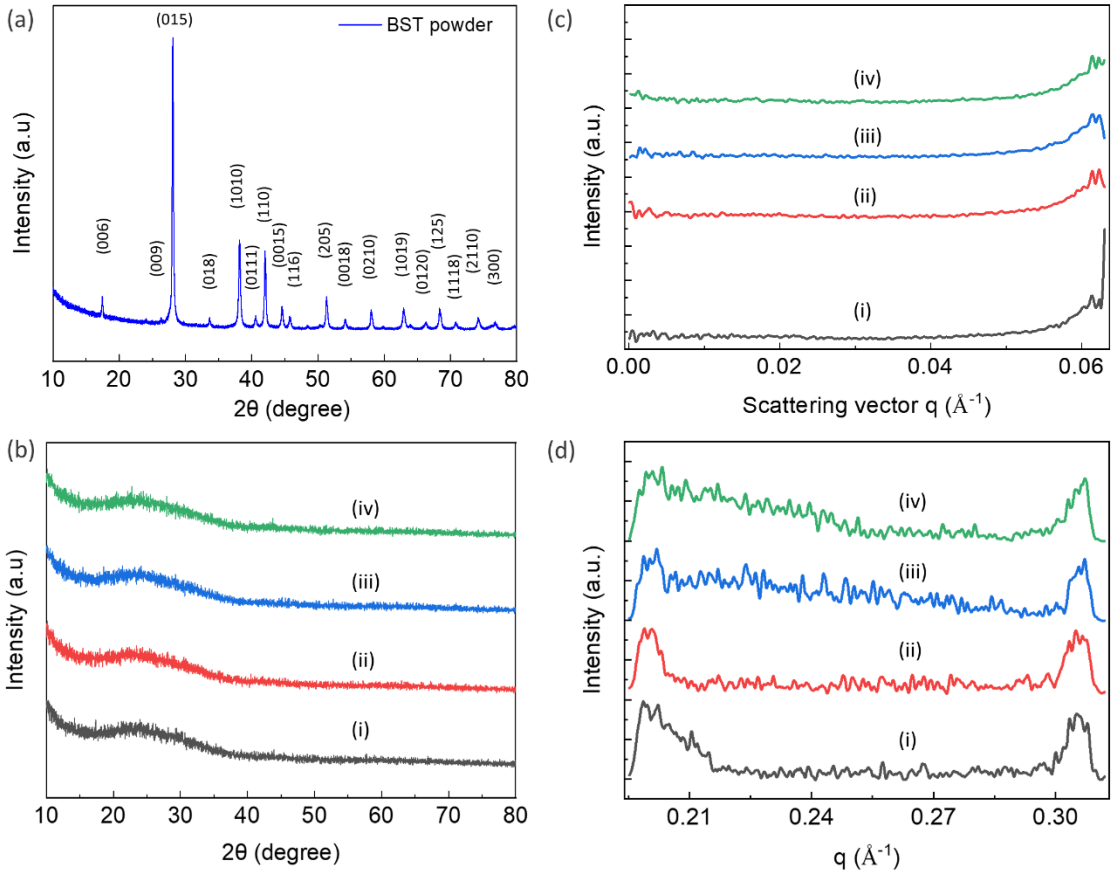

Figure S22. (a) XRD patterns of BST powder, and (b) XRD, (c) SAXS, and (d) WAXS patters of polymeric thin films including (i) pristine PEDOT:PSS, (ii) pristine PEDOT:PSS/40 wt% BST, (iii) 0.5 M H_2SO_4-0.1 M NaOH post-treated PEDOT:PSS, and (iv) 0.5 M H_2SO_4-0.1 M NaOH post-treated PEDOT:PSS/40 wt% BST.

References

[1] Z. Fan, J. Ouyang, Thermoelectric properties of PEDOT: PSS, Advanced Electronic Materials, 5 (2019) 1800769.
[2] X. Li, R. Zou, Z. Liu, J. Mata, B. Storer, Y. Chen, W. Qi, Z. Zhou, P. Zhang, Deciphering the superior thermoelectric property of post-treatment-free PEDOT: PSS/IL hybrid by X-ray and neutron scattering characterization, npj Flexible Electronics, 6 (2022) 6.